Solar Energy Materials & Solar Cells 157 (2016) 867–873

Contents lists available at ScienceDirect

Solar Energy Materials & Solar Cells

journal homepage: www.elsevier.com/locate/solmat

Photovoltaic effect in earth abundant solution processed Cu_2MnSnS_4 and $Cu_2MnSn(S,Se)_4$ thin films

Rajiv Ramanujam Prabhakar [a,b], Su Zhenghua [a], Zeng Xin [a], Tom Baikie [a], Leow Shin Woei [a], Sudhanshu Shukla [a], Sudip K. Batabyal [a], Oki Gunawan [c], Lydia Helena Wong [a,b,*]

[a] Energy Research Institute, Nanyang Technological University, Singapore
[b] School of Materials Science and Engineering, Nanyang Technological University, Singapore
[c] IBM T.J. Watson Research Center, Yorktown Heights, NY 10598, USA

ARTICLE INFO

Article history:
Received 3 September 2015
Received in revised form
21 May 2016
Accepted 4 July 2016
Available online 17 August 2016

Keywords:
Earth Abundant materials
Thin film
Photovoltaics
Cu_2MnSnS_4
$Cu_2MnSn(S,Se)_4$

ABSTRACT

In this work, we present the first report on thin film solar cells that employ Cu_2MnSnS_4 (CMTS) and $Cu_2MnSn(S, Se)_4$ (CMTSSe) as the absorber. CMTS and CMTSSe thin films are fabricated using a low cost spray pyrolysis technique in ambient atmosphere using water as a solvent. The crystal structure of the materials are similar to the established kesterite type photovoltaic materials such as $Cu_2ZnSn(S, Se)_4$ (CZTSSe). The bandgap of these materials is between 1.4 – 1.7 eV, which is ideal for optimum solar absorption and can be tuned by varying the ratio of the elemental constituents. The photovoltaic device with a structure of Mo/CMTS/CdS/TCO/top electrode is fabricated as a proof-of-concept and yields a power conversion efficiency of ~0.73% for the best optimized CMTS device with Na doping. Through analysis of the device characteristics, we identify a key problem of very high carrier density in the CMTS/CMTSSe absorber that leads to short collection length, low V_{oc}, low quantum efficiency at long wavelength and high shunt conductance that quench the fill factor. We also discuss several routes to improve the device performance.

1. Introduction

Thin film solar cells based on earth abundant materials have attracted a great deal of attention as they have the potential to generate the terawatts of electricity required to meet the global energy demands [1]. This class of materials consists of metal oxides, sulphides and phosphides such as FeS_2, Cu_2O, Zn_3P_2 and $Cu_2ZnSn(S, Se)_4$ (CZTSSe) [2]. Among these the power conversion efficiencies of FeS_2, Cu_2O and Zn_3P_2 thin films have been limited to less than 5% [3–5]. The most promising are CZTSSe based solar cells, where power conversion efficiencies (PCE) of greater than 12% have been achieved [6]. This also opens up the possibility of exploring materials with similar crystal structures and band gaps as CZTS/CZTSSe like Cu_2MSnS_4 (where M = Fe, Mn, Co and Ni) [7]. Among these metals (M), Mn is a potential replacement of Zn as it is more abundant than the latter and could be a potential absorber material for earth abundant thin film photovoltaics [8]. There is also another key motivation: in CZTSSe based solar cells, the Cu–Zn antisite defects such as [Cu_{Zn}^{-} + Zn_{Cu}^{+}] are suspected to be abundant, as they are next to each other in periodic table, which lead to severe potential fluctuations and tail states [9]. A severe tail states in CZTSSe is one of the dominant factors responsible for low open circuit voltage (V_{oc}), which is the biggest challenge with current CZTSSe technology. Hence, replacement of Zn with other metals could provide a route to alter the defects and tail states in the absorber and to eventually improve the V_{oc} [10].

Single crystals of Cu_2MnSnS_4 have been shown to have a stannite crystal structure, which have been shown to exhibit antiferromagnetism [11]. However the optical properties of such crystals have not been explored so far. Nanocrystals of CMTS have been synthesized by Cui et al. and Liang et al. and their bandgaps have been reported between 1.1 and 1.3 eV [7,12,13]. Despite having bandgaps in the range of ideal solar absorption, which according to Shockley-Queisser limit can yield PCE of ~33% for E_g = 1.15 and 1.34 eV (using AM 1.5 G spectrum), there have been no reports on the photovoltaic effect in CMTS [14,15]. Therefore the development of CMTS as an absorber in earth abundant thin film solar cells is important for the photovoltaic community owing to its similar crystal structure and bandgaps with CZTS/CZTSSe and increased abundance of Mn in comparison to Zn.

In this work, we report for the first time, the photovoltaic effect of Cu_2MnSnS_4 (CMTS) and $Cu_2MnSn(S, Se)_4$ (CMTSSe) using thin film solar cell configuration. The absorber films were prepared by

* Corresponding author at: School of Materials Science and Engineering, Nanyang Technological University, Singapore.
E-mail address: lydiawong@ntu.edu.sg (L.H. Wong).

http://dx.doi.org/10.1016/j.solmat.2016.07.006
0927-0248/

simple water based spray pyrolysis technique. This was followed by sulfurization and selenization to improve its crystallinity and facilitate grain growth. X-ray diffraction (XRD) and Raman spectroscopy confirmed the formation of the CMTS and CMTSSe phase. Power conversion efficiencies of ~ 0.07% have been achieved with CMTSSe and was further improved in CMTS (0.19%). CMTSSe exhibited a higher J_{sc} due to its lower bandgap. However CMTS exhibited a much higher photovoltage (236 mV) in comparison to CMTSSe (52 mV) partly due to higher band gap. The CMTSSe device exhibited a higher shunt conductance than the CMTS device which accounts for its lower fill factor. Upon optimizing the film thickness and doping with Na, the efficiency of CMTS device was further improved to 0.73%. The current results show the great potential of CMTS and CMTSSe as absorber in thin film solar cells based on earth abundant materials.

2. Experimental section

2.1. Synthesis of CMTS thin films by spray pyrolysis

Cu_2MnSnS_4 thin films were prepared by spray pyrolysis (Holmarc Optomechatronics Pvt Ltd) in ambient atmosphere (50 mins spraying time). The precursor solutions used were $CuCl_20\cdot 2H_2O$ (0.2 M), $MnCl_20\cdot 2H_2O$ (0.1 M), $SnCl_20\cdot 2H_2O$ (0.1 M) and Thiourea (1 M) with DI water as the solvent. These precursors were taken in Cu-poor, Mn rich composition of Cu_2MnSnS_4 (thiourea was taken in excess to compensate for the sulphur loss during the spraying) and sprayed onto Mo coated glass substrates on a hot plate at a temperature of 300–400 °C. For Na doping, NaCl was mixed along with the precursor solution.

2.2. Sulphurization and selenization

After the thin films were prepared by spray pyrolysis, the samples were annealed in a horizontal tube furnace at a temperature of 500–550 °C and in the presence of sulphur (150 mg and time =30 min) and selenium (50 mg and time =20 min) to prepare CMTS and CMTSSe respectively in an argon atmosphere. After sulphurization and selenization the thickness of films for CMTS and CMTSSe were ~ 1.2 and 1.3 μm respectively. These films were used from SEM, XRD, Raman and solar cell fabrication.

2.3. Morphology, crystal structure and optical properties

Scanning Electron Microscopy images were obtained using a Field Emission Scanning Electron Microscope (FESEM), JEOL JSM-7600F. Phase identification was investigated using a X-ray Diffraction (XRD) by Bruker D8 Advance Diffractometer. Data fitting of the diffraction patterns was performed using the software Topas Version 3 with the lattice parameters of the respective CMTS/Se samples extracted from the data using a Pawley fit technique. Micro Raman spectroscopy was performed using a Renishaw system 2000 (excitation wavelength 514 nm and laser spot size 2 μm). Thin films of CMTS and CMTSSe were exfoliated from Mo for AC Hall measurements (during exfoliation a small part of the film was attached to the Mo). Reflectivity measurements were obtained using a UV–Vis spectrophotometer (Shimadzu UV-3600).

2.4. Fabrication of solar cells

CMTS and CMTSSe thin films (thickness 1.2–1.3 μm) was used for solar cell fabrication. Firstly, CdS buffer layer (50 nm) was deposited on prepared CMTS/Mo/SLG at 80 °C for 10 min using chemical bath deposition (CBD). The chemical bath consisted of deionized H_2O (140 mL), NH_4OH (28–30%, 20 mL), 0.15 M $CdSO_4$ (20 mL, AR) and 0.75 M thiourea (20 mL, AR). Next, 50 nm i-ZnO followed by 500 nm ZnO:Al layer were deposited by RF and DC magnetron sputtering.. The target composition of AZO is ZnO (98% wt) and Al_2O_3 (2% wt), the sputtering power density is DC 4.3 w/cm^2 and the pressure is 0.5 Pa. Finally Silver ink was printed on Al: ZnO layer to form top contact fingers. The area of the device fabricated was 0.15 cm^2.

2.5. Characterization of solar cells

A solar simulator (VS-0852) was utilized to measure the J-V characteristics of solar cells under the simulated AM 1.5 100 mW cm^{-2} illumination using a Keithley Source (2612 A) meter and IV tester software package. The solar simulator was equipped with a 500 W xenon lamp and the light intensity was calibrated using Si reference solar cell (Fraunhofer). External quantum efficiency (EQE) spectra were measured with a spectral resolution of 1 nm using a PVE300 photovoltaic device characterization system (Bentham) equipped with a xenon/quartz lamp.

3. Results and discussion

Fig. 1 shows the XRD patterns of the CMTS and CMTSSe thin films after sulphurization and selenization respectively. In Fig. 1 the diffraction reflections are indexed in a tetragonal cell, in the space group *I*-42*m*, with the reflections corresponding to the (112), (200), (220) and (312) planes observed and an enhancement of the (112) plane suggestive of a preferred crystallite orientation for CMTS (red curve). The extracted lattice parameters for CMTS (a=5.492(1) Å, c=10.824(3) Å and cell volume=326.5 Å^3(3)) are in close agreement with the reported values in literature [16]. Similarly, the pattern for CMTSSe (JCPDS 00-026-0542) (blue curve) is also indexed in a tetragonal cell (space group $I-42$ m) and the reflections corresponding to the (112), (220) and (312) planes are observed. The preferred crystallite orientation in CMTSSe also shows an enhanced intensity of the (112) reflection. As expected, a shift in the reflection positions of the CMTSSe towards lower 2θ values is observed, due to the substitution of S^{2-} (IR=1.84 Å) with the larger Se^{2-} ions (IR=1.98) [17]. The extracted lattice parameters for CMTSSe are a=5.59 Å (1) Å, c=11.04(3) Å, cell volume (357.6(3) A^3), where both the a and c axes increase in comparison to CMTS. The crystallite size is estimated using the Scherrer formula and the Williamson- Hall approach and the crystallite size of CMTS is found to be(~ 30 nm) smaller than the CMTSSe (57 nm) [18]. Fig. 2(A) shows the Raman spectrum of CMTS thin film with one strong peak at 327 cm^{-1} and a shoulder peak at 343 cm^{-1}. The peak at 327 cm^{-1} corresponds to the A1 vibration mode and the shoulder peak at 343 cm^{-1} was also observed in Cu_2MnSnS_4 [19]. This further confirms the presence of CMTS phase and shows the absence of any impurity phases. Fig. 2(B) shows the Raman spectrum of CMTSSe and it is characterized by two prominent peaks. Due to the partial replacement of Sulphur atoms by Se atoms, the frequency of the A1 mode has been shifted to lower frequencies due to the higher atomic mass of Se [20]. In addition, since the cell volume of CMTSSe is larger than CMTS (as shown from XRD analysis), the bond-stretching force is lower in CMTSSe. Therefore a combination of higher atomic mass of Se and the decreased bond-stretching force results in the shifting of A1 modes towards lower frequencies. Fig. 2(C) and (D) show the cross sectional SEM images of the CMTS and CMTSSe thin films after sulphurization and selenization. It is evident from the SEM image that the grain size is larger in CMTSSe in comparison to CMTS as selenization has been shown to improve grain size [21]. EDX (Energy Dispersive X-Ray Spectroscopy) spectrum shows the presence of all metals (Cu, Mn, Sn) for both CMTS and CMTSSe

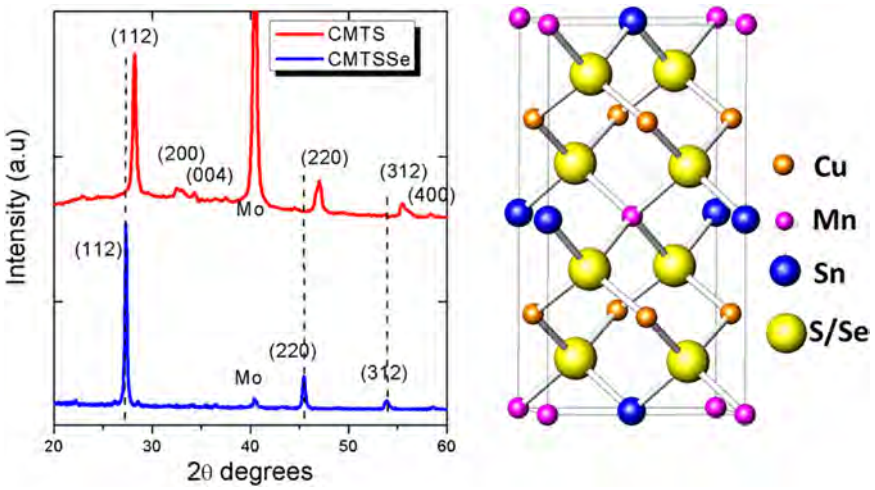

Fig. 1. XRD patterns of CMTS [16] and CMTSSe (JCPDS 00-026-0542) thin films after sulphurization and selenization respectively. A shift was observed in the diffraction peaks upon incorporation of Se into CMTS. (For interpretation of the references to color in this figure, the reader is referred to the web version of this article.)

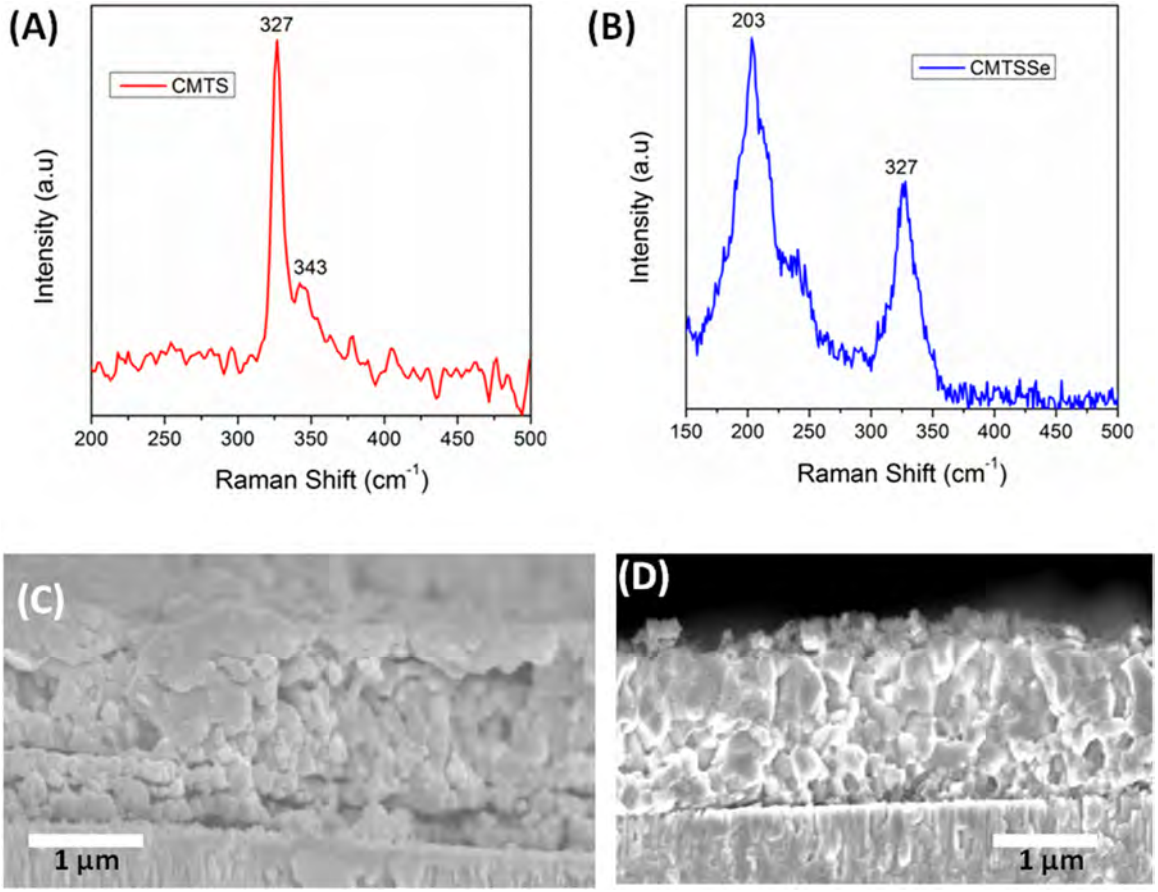

Fig. 2. Raman spectrum of **(A)** CMTS and **(B)** CMTSSe. Cross sectional SEM images of **(C)** CMTS **(D)** CMTSSe.

(Supporting information S1). The stoichiometry data for CMTS and CMTSSe was obtained from SEM – EDX (Fig. S1(C)) and it was found to be CMTS- $Cu_{1.57}Mn_{0.90}Sn_{0.73}S_{4.78}$ and CMTSSe – $Cu_{1.69}Mn_{0.97}Sn_{1.01}S_{1.4}Se_{2.9}$. The sulphur to selenium ratio for the CMTSSe is ~ 0.48.

Fig. 3(a) and (b) show the J-V curves of the CMTS and CMTSSe thin film solar cells under AM1.5 illumination. The best CMTS device exhibits a power conversion efficiency of 0.19% which is higher than the best CMTSSe device (0.07%). Table 1 shows the average power conversion efficiency obtained for CMTS device (0.16%) and CMTSSe device (0.05%) with standard deviation. Fig. S2 (supporting information) shows the cross section SEM image of the CMTS device. The V_{oc} of CMTS device (236 mV) is much higher in comparison to the CMTSSe device (52 mV). However the J_{sc} of CMTS (2.22 mA/cm^2) is lower than CMTSSe (5.1 mA/cm^2). In order to comprehend the J_{sc} trends, the quantum efficiency curves of the CMTS and CMTSSe device are investigated. Fig. 4(A) and (B) show the external quantum efficiency vs wavelength plots for the two devices. From the [E x ln(1-EQE)]^2 vs E plots the band gaps are calculated and CMTS (1.60 eV) has a higher band gap than CMTSSe

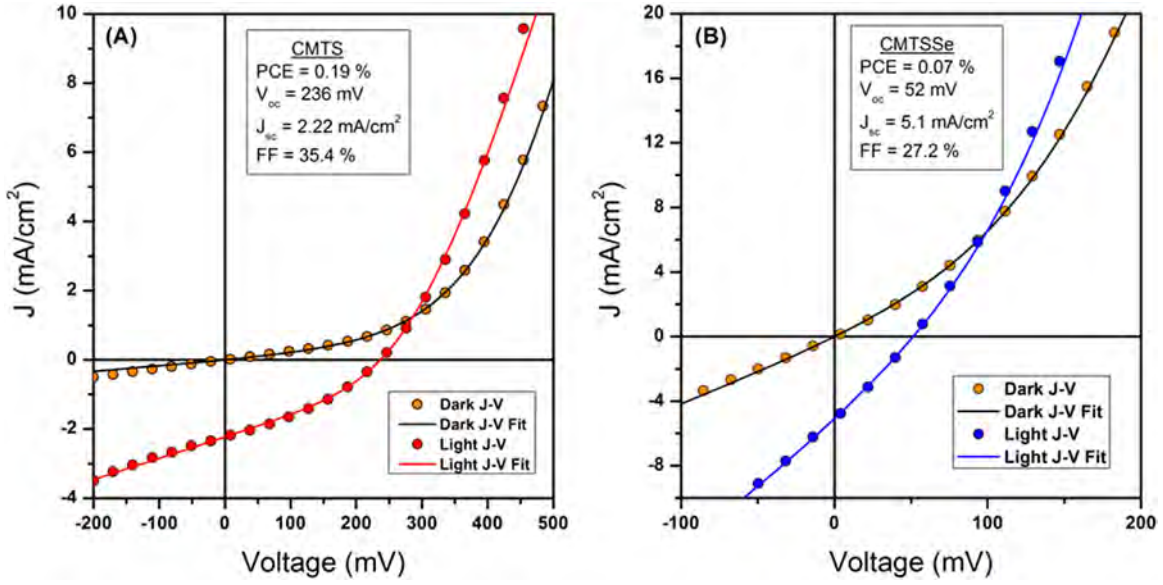

Fig. 3. Light and dark J-V of (A) CMTS and (B) CMTSSe solar cell under simulated AM1.5 1 sun illumination. Data points are the measurement and the solid lines are the four-diode-parameter model fit as detailed in Table 1.

Table 1
Device characteristics of the CMTS and CMTSSe including the diode parameters: ideality factor n, reverse saturation current J_0, series resistance R_S, and shunt conductance G_S, extracted using Lambert-W fitting method [23]. The parameters in parentheses are from dark J-V curves. The average and standard deviations of the photovoltaic parameters (Efficiency, Fill factor, V_{oc} and J_{sc}) for CMTS and CMTSSe are also provided.

Device	Eff (%)	FF (%)	V_{oc} (mV)	J_{sc} (mA/cm^2)	E_g (eV)	V_{oc}, def	n	J_0 (A/cm^2)	R_s (Ohm cm^2)	G_s (mS/cm^2)
CMTS (champion)	**0.19**	**35.4**	**236**	**2.22**	**1.6**	**1.364**	**1.76 (1.88)**	**5.38×10^{-6} (1.03×10^{-6})**	**14.6 (17.6)**	**6.12 (2.53)**
CMTSSe (Champion)	**0.07**	**27.2**	**52**	**5.1**	**1.47**	**1.418**	**1.83 (1.66)**	**7.87×10^{-4} (3.56×10^{-4})**	**1.11 (2.8)**	**79.4 (41.4)**
CMTS										
Avg	**0.16**	**34**	**225**	**2.04**						
Stdev	**0.022**	**0.008**	**12.01**	**0.155**						
CMTSSe										
Avg	**0.05**	**0.27**	**44**	**4.66**						
Stdev	**0.018**	**0.005**	**10**	**0.33**						

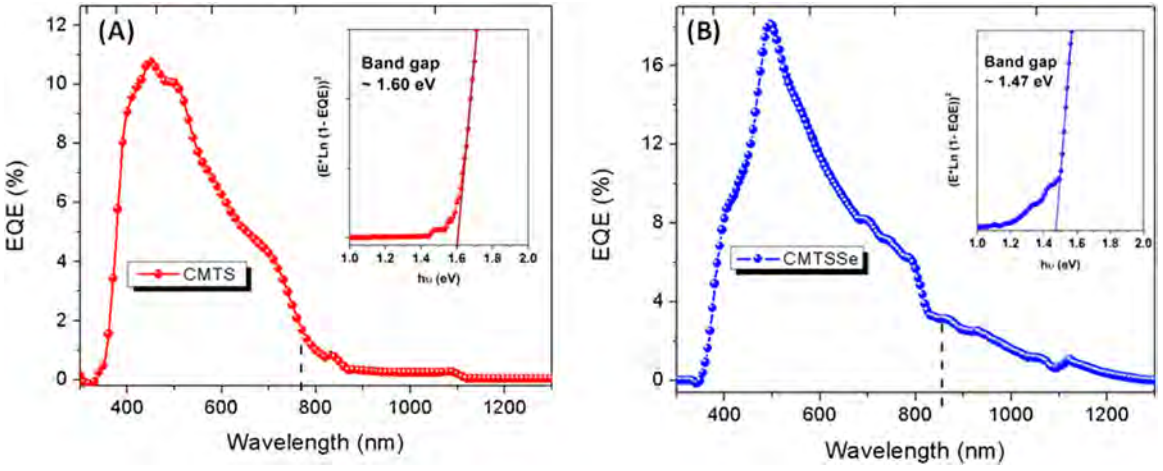

Fig. 4. EQE curves of (A) CMTS and (B) CMTSSe solar cells (Inset shows the band gap estimate from $E^*Ln(1\text{-}EQE)^2$ vs E plots).

(1.47 eV). This could account for the increased J_{sc} of the CMTSSe device. For the CMTS device, the EQE curves show a weak response at the red portion of the spectrum ($\lambda > 600$ nm) which indicates a low collection efficiency. This could be due to high recombination losses in the bulk and depletion region that limits the minority carrier lifetime [22]. Even though similar trend is observed for CMTSSe device, the onset of the EQE curve is shifted to higher wavelength (red shift) in comparison to CMTS device due to its lower band gap. To understand the quality of the *p-n* junction, we extract the diode parameters (n, J_0, R_S, G_S) of the light and dark J-V curves of the CMTS and CMTSSe (Fig. 3, Table 1). The detailed device parameters including the four diode parameters (ideality

factor n, reverse saturation current J_0, series resistance R_S, and shunt conductance G_S,) are presented in Table 1 obtained using the Lambert-W fitting method [23]. It is evident from the dark curves that the CMTSSe has a nearly ohmic behavior and exhibits a poorer rectification than the CMTS dark J-V curves. Overall both devices show very high dark shunt conductance G_S which could be due to very high carrier density absorber or electrical shunt due to film non-uniformity. Furthermore G_S becomes more severe (higher) under light condition which indicates voltage-dependent-collection-efficiency problem i.e. current collection that increases with more negative bias [24]. This suggests a very short collection length (approximately equal to the sum depletion width and minority carrier diffusion length) - specifically where the diffusion length is smaller than the depletion width. In this case, the collection length is strongly modulated by the change in the depletion width under change in voltage bias. This situation occurs in high carrier density absorber where the minority carrier lifetime is very short and thus the minority carrier diffusion length is short. The fill factors (FF) of CMTS (35.4%) is higher than that of CMTSSe (27.2%) as a result of lower G_S and higher V_{oc} of the former cell. Despite these issues, the ideality factors in these devices show promising low values of ~1.8, within the range of ideality factors of good CIGSSe or CZTSSe solar cells (1.3–2.0) [25]. A severe low cross-over of the light and dark I-V curves in both CMTS and CMTSSe devices was observed as shown in Fig. 3. This behavior often occurs in low efficiency thin film devices that could be caused by few factors such as the voltage-dependent-collection-efficiency problem discussed above or due to the photoconductivity effect of the CdS [26].

The key information of the absorber film that determines the photovoltaic performance of the device are carrier density and mobility. For this purpose we exfoliate the same CMTS and CMTSSe films (0.55 μm thick, grown on Mo/glass) and transfer them to a secondary substrate for Hall measurements. However, due to low carrier mobility we employ a newly developed technique of high sensitivity Hall measurement using rotating parallel dipole line (PDL) system. The system consists of a rotating master and slave dipole line magnet [Fig. 5(a)] as described in reference [27,28]. Here we capture the ac magnetic field and the raw (transverse) Hall resistance and calculate their corresponding power spectral density (PSD) spectra. The PSD of the Hall signal shows the desired frequency content [Fig. 5(e)] and subsequently

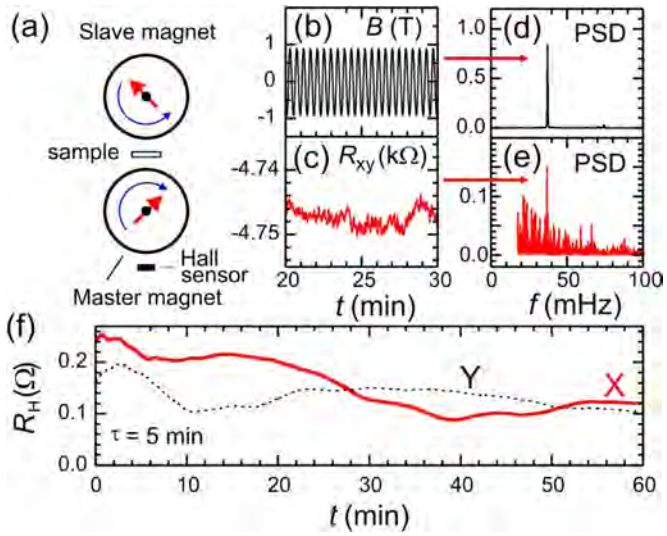

Fig. 5. Rotating PDL Hall measurement [27,28] on exfoliated CMTS film: (a) Experimental Setup. (b) Magnetic field (B) oscillation. (c) Raw Hall signal (R_{xy}). (d) Power spectral density (PSD) spectrum of B. (e) PSD of (R_{xy}). (f) Numerical lock-in output showing the desired Hall signal (X) and parasitic emf signal (Y).

we perform lock-in analysis to obtain the final Hall signal (the in-phase signal X). The Hall measurements on the exfoliated CMTS (CMTSSe) samples yield signs that confirm p-type carrier with density of $p = 8.4 \times 10^{19}/\text{cm}^3$ ($3.8 \times 10^{19}/\text{cm}^3$) and mobility $\mu = 0.16\ \text{cm}^2/\text{Vs}$ ($1.4\ \text{cm}^2/\text{Vs}$). Thus the Hall measurements reveal that the carrier density of the film is too high for an optimum solar absorber. Such a metallic film has a very narrow depletion width leading to very low collection efficiency or low J_{sc} and high shunt conductance. The light dependent shunt conductance observed in CMTS and CMTSSe (Fig. 3) was also due to highly metallic nature of these films which is supported by Hall measurements (Carrier density $10^{19}\ \text{cm}^{-3}$). The high carrier density in the absorber leads to very narrow depletion width, which in turns induces voltage-dependent-collection-efficiency problem, where the current collection increases at reduced voltage. This effects results in higher shunt conductance under light condition versus that in dark. It also usually has very short minority lifetime (due to enhanced Auger recombination process) and thus lead to low open circuit voltage - all these consistent with the experimental observation. This high carrier density is the key problem in our current generation of CMTS/CMTSSe devices; thus a critical strategy for performance improvement is to reduce the carrier density in future devices to a range of $10^{15} - 10^{16}/\text{cm}^3$ like in high performance CIGSSe and CZTSSe [6,29].

Defect passivation and grain growth strategies such as doping with Na could reduce the recombination in CMTS and hence increasing the power conversion efficiency of CMTS [30]. Na was incorporation into CMTS by doping with NaCl during the spray process in order to improve grain growth and reduce non-radiative recombination in CMTS. With Na doping grain growth was observed in CMTS (Fig. S3(A) and (B)). XRD and Raman spectra indicate that the phase of CMTS was unaffected by the incorporation of Na (Fig. S3(C) and (D). By Na doping and optimizing the thickness of CMTS absorber, significant improvement in the power conversion efficiencies of CMTS was observed. Power conversion efficiencies of ~ 0.73% was obtained with significant improvements in the J_{sc} (4.95 mA/cm2) and V_{oc} (381 mV) (Fig. 6(A)). In order to understand the improvement in the J_{sc}, EQE spectra were obtained which revealed increased charge collection in the longer wavelength region (Fig. 6(B)). The band gap of Na doped CMTS was extracted from the EQE curve (Inset of Fig. 6(B)) ~ 1.61 eV similar to undoped CMTS.

The decay of the internal quantum efficiency (IQE) curve below the band gap could shine light upon the electrostatic potential fluctuations in the absorber. The IQE curve is obtained from the reflectivity spectrum of the full CMTS device. Electrostatic potential fluctuations in a semiconductor are very important particularly when considering its application in photovoltaics [9]. From the mode l developed by Shklovskii and Efros [31], the absorption coefficient below the band gap for photon energies close to the band gap, could be related by the following equation

$$\alpha \propto exp\left(\frac{-2}{5\sqrt{\pi}}\frac{E_g - \hbar\omega}{\gamma/2}\right) \quad (1)$$

Where E_g is the band gap, $\hbar\omega$ is the photon energy and γ is the amplitude of potential fluctuations. Since the IQE curve is determined by the absorption coefficient and the collection efficiency in the solar cell, the absorption coefficient can be obtained from the IQE curve using the following relationship

$$\alpha \propto -\ln\ (1 - IQE(\hbar\omega)) \quad (2)$$

which is derived from using a small IQE approximation (IQE < 0.3) [9,32]. Upon plotting the absorption coefficient versus photon energy and fitting it with Eq. (2), the amplitude of potential fluctuations (γ) can be obtained and for CMTS it is found to be around

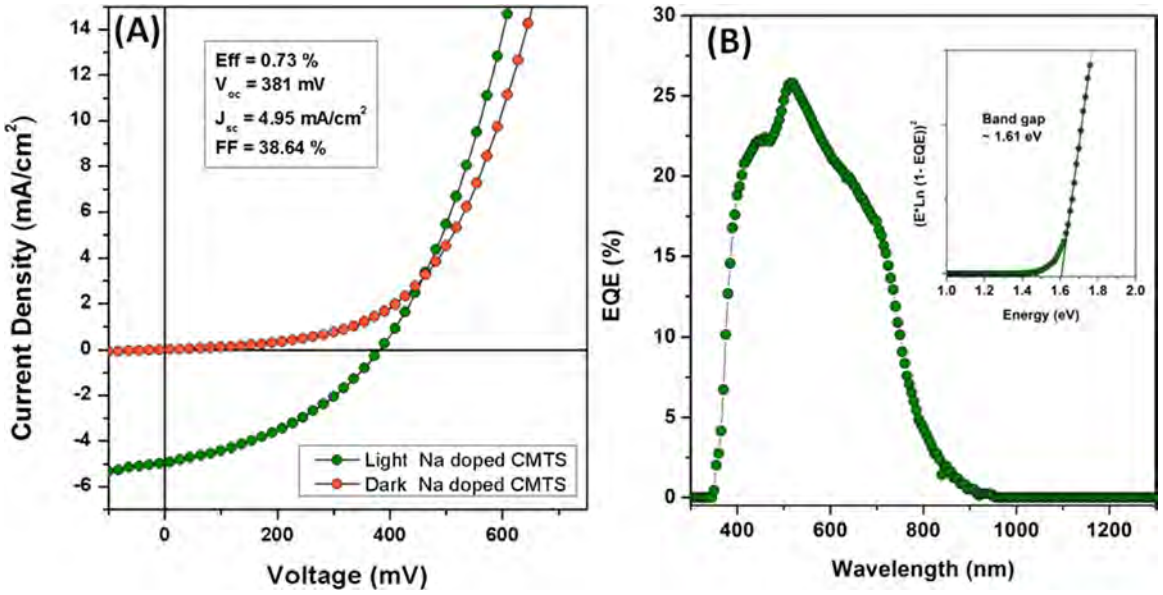

Fig. 6. **(A)** J-V curves of optimized Na doped CMTS **(B)** EQE curve of the optimized Na doped CMTS (Inset shows the band gap ~ 1.61 eV).

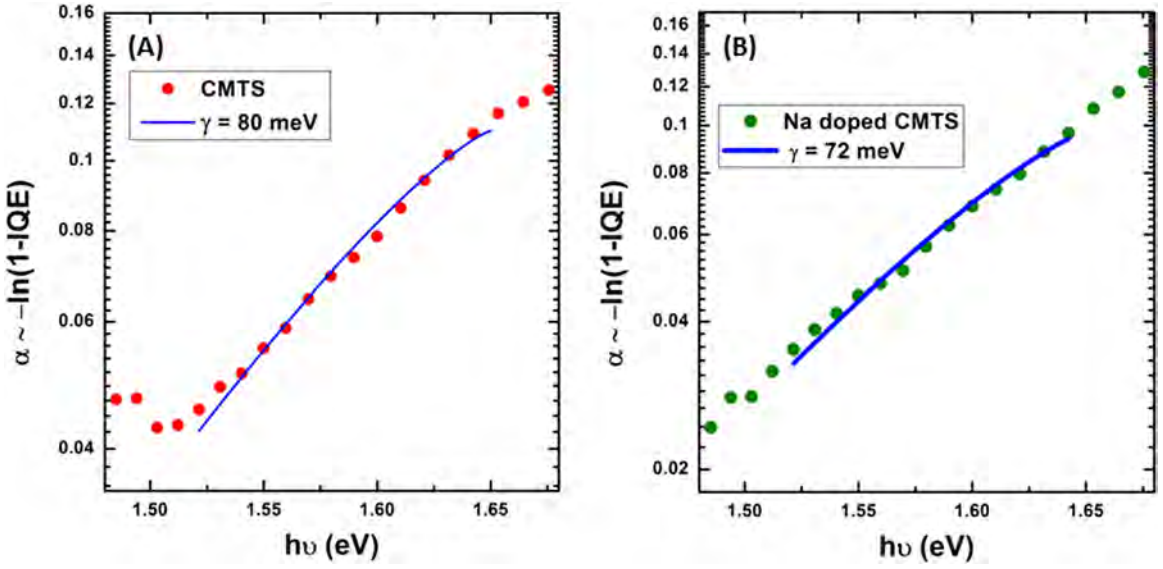

Fig. 7. Absorption coefficient (obtained from –ln(1-IQE)) vs energy plots at below band gap excitation for (A) CMTS (B) optimized Na doped CMTS.

80 meV (Fig. 7(A)). However the Na doped CMTS had a γ value of 72 meV indicating that the amplitude of potential fluctuations was lower in Na doped CMTS which could explain the improvement in the V_{oc} of Na doped CMTS device (Fig. 7(B). This is however higher in comparison to CZTSSe (56.4 meV) and CIGSSe (35.5 meV) [9]. This higher degree of potential fluctuation also leads to lower V_{oc} and often related to low carrier mobility, consistent with the Hall measurement above. Therefore the fundamental understanding of the nature of defects and the defects that cause potential fluctuations is needed to improve the power conversion efficiencies of CMTS in the future. The V_{oc} deficit (V_{oc}, def$=E_g/q-V_{oc}$) can provide useful information regarding the electronic quality of the solar cell absorber [33]. The V_{oc} deficit of CMTS (1.36 eV) and Na doped CMTS (1.23 eV) is lower than CMTSSe (1.41 eV) which shows that the recombination losses (due to deep defects and interfaces) is probably lower in CMTS [34]. The influence of Na doping on the electrical properties and recombination mechanisms of CMTS is currently in progress and will be published elsewhere.

Finally the power conversion efficiencies of CMTS(Se) solar cells obtained in this paper are very promising and could open up new possibilities in earth abundant thin film photovoltaics. It should be noted that the first reported power conversion efficiency of CZTS was 0.66% by Katagiri et al. in 1997 [35]. Currently the record efficiencies for CZTS solar cells is 12.6%. CMTS has similar band gaps with CZTS and power conversion efficiencies as high as ~ 30% is theoretically possible based on the Shockley-Quiesser limit. By optimizing the buffer layers and the electrical properties of the absorber layer (by tuning carrier density), we believe that the efficiencies of the current CMTS solar cells could be further improved and this will be investigated in the future.

4. Conclusion

Photovoltaic effect of CMTS and CMTSSe thin films are shown for the first time. The thin films are synthesized using spray pyrolysis followed by sulphurization and selenization. XRD and Raman analysis reveal the formation of the CMTS and CMTSSe phase.

The power conversion efficiencies of CMTS and CMTSSe devices are 0.19% and 0.07%, respectively. Although J_{sc} is higher in CMTSSe device due to its lower band gap, CMTS results in a higher overall power conversion efficiency due to its lower shunt conductance and larger V_{oc}. The V_{oc} deficit of CMTS is marginally lower than CMTSSe device thus indicating lesser recombination in CMTS. The high carrier concentration in these films is identified as the major factor in the high V_{oc} deficit and low FF problem (due to high shunt conductance). Low majority carrier (hole) mobility ($\mu = 0.2 - 1.4$ cm^2/Vs) is also found to contribute to high series resistance and again low FF. The optimized Na doped CMTS resulted in higher efficiency (0.73%) owing to its improved charge collection in the longer wavelength region and reduced potential fluctuations. Finally, this first demonstration of photovoltaic effect of CMTS and CMTSSe may lead to the use of these materials in different configuration of solar cells such as thin films, mesoporous sensitized solar cells, etc.

Acknowledgments

This work is supported by Singapore -Berkeley Research Initiative for Sustainable Energy (SinBeRISE) CREATE Programme under the Campus for Research Excellence and Technological Enterprise (CREATE), that is supported by the National Research Foundation, Prime Minister's Office, Singapore, and Energy Innovation Research Programme grant number NRF2011EWT-CERP001-019.

Appendix A. Supplementary material

Supplementary data associated with this article can be found in the online version at http://dx.doi.org/10.1016/j.solmat.2016.07.006.

References

[1] Y.S. Lee, M. Bertoni, M.K. Chan, G. Ceder, T. Buonassisi, Earth abundant materials for high efficiency heterojunction thin film solar cells, in: Proceedings of the 34th IEEE Photovoltaic Specialists Conference (PVSC), 2009 , pp. 002375–002377.
[2] C. Wadia, A.P. Alivisatos, D.M. Kammen, Materials availability expands the opportunity for large-scale photovoltaics deployment, Environ. Sci. Technol. 43 (2009) 2072–2077.
[3] J.P. Bosco, D.O. Scanlon, G.W. Watson, N.S. Lewis, H.A. Atwater, Energy-band alignment of II-VI/Zn3P2 heterojunctions from X-ray photoemission spectroscopy, J. Appl. Phys. 113 (2013) 203705.
[4] N. Berry, M. Cheng, C.L. Perkins, M. Limpinsel, J.C. Hemminger, M. Law, Atmospheric-pressure chemical vapor deposition of iron pyrite thin films, Adv. Energy Mater. 2 (2012) 1124–1135.
[5] S.W. Lee, Y.S. Lee, J. Heo, S.C. Siah, D. Chua, R.E. Brandt, S.B. Kim, J.P. Mailoa, T. Buonassisi, R.G. Gordon, Improved Cu_2O-based solar cells using atomic layer deposition to control the Cu oxidation state at the p-n junction, Adv. Energy Mater. 4 (2014) 1301916.
[6] W. Wang, M.T. Winkler, O. Gunawan, T. Gokmen, T.K. Todorov, Y. Zhu, D. B. Mitzi, Device characteristics of CZTSSe thin-film solar cells with 12.6% efficiency, Adv. Energy Mater. 4 (2014) 1301465.
[7] Y. Cui, R. Deng, G. Wang, D. Pan, A general strategy for synthesis of quaternary semiconductor Cu_2MSnS_4 (M = Co2+, Fe2+, Ni2+, Mn2+) nanocrystals, J. Mater. Chem. 22 (2012) 23136–23140.
[8] T. Unold, H.W. Schock, Nonconventional (Non-silicon-based) photovoltaic materials, Annu. Rev. Mater. Res. 41 (2011) 297–321.
[9] T. Gokmen, O. Gunawan, T.K. Todorov, D.B. Mitzi, Band tailing and efficiency limitation in kesterite solar cells, Appl. Phys. Lett. 103 (2013) 103506.
[10] A. Polizzotti, I.L. Repins, R. Noufi, S.-H. Wei, D.B. Mitzi, The state and future prospects of kesterite photovoltaics, Energy Environ. Sci. 6 (2013) 3171–3182.
[11] T. Fries, Y. Shapira, F. Palacio, M.C. Morón, G.J. McIntyre, R. Kershaw, A. Wold, E. J. McNiff, Magnetic ordering of the antiferromagnet Cu_2MnSnS_4 from magnetization and neutron-scattering measurements, Phys. Rev. B 56 (1997) 5424–5431.
[12] X. Liang, P. Guo, G. Wang, R. Deng, D. Pan, X. Wei, Dilute magnetic semiconductor Cu_2MnSnS_4 nanocrystals with a novel zincblende and wurtzite structure, RSC Adv. 2 (2012) 5044–5046.
[13] L. Shi, Y. Li, C. Wu, R.-K. Zheng, Preparation and photoelectric and magnetic properties of Cu_2MnSnS_4 nanosheets, ChemPlusChem 80 (2015) 1537–1540.
[14] W. Shockley, H.J. Queisser, Detailed balance limit of efficiency of p-n junction solar cells, J. Appl. Phys. 32 (1961) 510–519.
[15] U. Rau, J.H. Werner, Radiative efficiency limits of solar cells with lateral band-gap fluctuations, Appl. Phys. Lett. 84 (2004) 3735–3737.
[16] F. López-Vergara, A. Galdámez, V. Manríquez, P. Barahona, O. Peña, $Cu_2Mn_{1-x}Co_xSnS_4$: novel këwhile type solid solutions, J. Solid State Chem. 198 (2013) 386–391.
[17] R. Shannon, Revised effective ionic and radii systematic studies of interatomic distances in halides and chalcogenides, Acta Crystallogr. Sect. A 32 (1976) 751–767.
[18] G.K. Williamson, W.H. Hall, X-ray line broadening from filed aluminium and wolfram, Acta Metall. 1 (1953) 22–31.
[19] M. Himmrich, H. Haeuseler, Far infrared studies on stannite and wurtzstannite type compounds, Spectrochim. Acta A: Mol. Spectroscopy 47 (1991) 933–942.
[20] J. He, L. Sun, S. Chen, Y. Chen, P. Yang, J. Chu, Composition dependence of structure and optical properties of $Cu_2ZnSn(S,Se)_4$ solid solutions: an experimental study, J. Alloy. Compd. 511 (2012) 129–132.
[21] K. Woo, Y. Kim, W. Yang, K. Kim, I. Kim, Y. Oh, J.Y. Kim, J. Moon, Band-gap-graded $Cu_2ZnSn(S_{1-x},Se_x)_4$ solar cells fabricated by an ethanol-based, particulate precursor ink route, Sci. Rep. 3 (2013) 3069.
[22] S. Ahmed, K.B. Reuter, O. Gunawan, L. Guo, L.T. Romankiw, H. Deligianni, A. High, Efficiency electrodeposited Cu_2ZnSnS_4 solar cell, Adv. Energy Mater. 2 (2012) 253–259.
[23] C. Zhang, J. Zhang, Y. Hao, Z. Lin, C. Zhu, A simple and efficient solar cell parameter extraction method from a single current-voltage curve, J. Appl. Phys. 110 (2011) 064504.
[24] S. Hegedus, D. Desai, C. Thompson, Voltage dependent photocurrent collection in CdTe/CdS solar cells, Prog. Photovolt.: Res. Appl. 15 (2007) 587–602.
[25] O. Gunawan, T. Gokmen, D.B. Mitzi, Device Characteristics of Hydrazine-Processed CZTSSe, in: K. Ito (Ed.), Copper Zinc Tin Sulfide-Based Thin-Film Solar Cells, John Wiley & Sons, 2015.
[26] A.O. Pudov, A. Kanevce, H.A. Al-Thani, J.R. Sites, F.S. Hasoon, Secondary barriers in CdS–$CuIn_{1-x}Ga_xSe_2$ solar cells, J. Appl. Phys. 97 (2005) 064901.
[27] O. Gunawan, Y. Virgus, K.F. Tai, A parallel dipole line system, Appl. Phys. Lett. 106 (2015) 062407.
[28] T.G.O. Gunawan, Hall measurement system with rotary magnet, in, US 9,041,389, 2015.
[29] I. Repins, M.A. Contreras, B. Egaas, C. DeHart, J. Scharf, C.L. Perkins, B. To, R. Noufi, 19·9%-efficient ZnO/CdS/$CuInGaSe_2$ solar cell with 81·2% fill factor, Prog. Photovolt.: Res. Appl. 16 (2008) 235–239.
[30] T. Gershon, B. Shin, N. Bojarczuk, M. Hopstaken, D.B. Mitzi, S. Guha, The role of sodium as a surfactant and suppressor of non-radiative recombination at internal surfaces in Cu_2ZnSnS_4, Adv. Energy Mater. 5 (2014) 1400849.
[31] B.I. Shklovskii, A.L. Efros, Electronic Properties of Doped Semiconductors, Springer-Verlag, Berlin, 1984.
[32] X.X. Liu, J.R. Sites, Solar cell collection efficiency and its variation with voltage, J. Appl. Phys. 75 (1994) 577–581.
[33] R.R. King, D. Bhusari, A. Boca, D. Larrabee, X.Q. Liu, W. Hong, C.M. Fetzer, D. C. Law, N.H. Karam, Band gap-voltage offset and energy production in next-generation multijunction solar cells, Prog. Photovolt.: Res. Appl. 19 (2011) 797–812.
[34] S. De Wolf, J. Holovsky, S.-J. Moon, P. Löper, B. Niesen, M. Ledinsky, F.-J. Haug, J.-H. Yum, C. Ballif, Organometallic halide perovskites: sharp optical absorption edge and its relation to photovoltaic performance, J. Phys. Chem. Lett. 5 (2014) 1035–1039.
[35] H. Katagiri, N. Sasaguchi, S. Hando, S. Hoshino, J. Ohashi, T. Yokota, Preparation and evaluation of Cu_2ZnSnS_4 thin films by sulfurization of EB evaporated precursors, Sol. Energy Mater. Sol. Cells 49 (1997) 407–414.